Materials Advances

ROYAL SOCIETY OF CHEMISTRY

PAPER

View Article Online
View Journal | View Issue

Cite this: *Mater. Adv.*, 2020, **1**, 2450

Effect of $AuBr_3$ additive on the scintillation properties of $BaBr_2$:Eu and $Cs_2LiLaBr_6$:Ce

Federico Moretti, * Dongsheng Yuan, *† Didier Perrodin and Edith Bourret

Received 23rd May 2020,
Accepted 16th September 2020

DOI: 10.1039/d0ma00340a

rsc.li/materials-advances

Following the observation of large increases in light output of BaBrCl:Eu single crystals using $AuBr_3$ as an additive in the melt, the impact of this process on the scintillation properties of other Br-based scintillating materials is investigated in an attempt to assess its broader use. Results for $Cs_2LiLaBr_6$:Ce and $BaBr_2$:Eu single crystals with various Ce and Eu concentrations are presented. The results indicate that such an additive has very different effects in the two investigated materials. Although $AuBr_3$ is not incorporated in the two crystalline matrices, it increases remarkably, by up to a factor 2, the light yield of $BaBr_2$:Eu in a similar manner to that observed for BaBrCl:Eu, but is at best ineffective in the case of $Cs_2LiLaBr_6$:Ce. The improvements detected in the case of $BaBr_2$:Eu are related to a substantial reduction in the long lived scintillation decay tails as well as in the thermally stimulated luminescence amplitude with respect to the crystal grown without $AuBr_3$ in the melt. These improvements are, however, associated with a reduction in the energy resolution of these crystals related to a worse energy response non-proportionality. In the case of $Cs_2LiLaBr_6$:Ce, no clear improvements in either the light yield or the scintillation decay time are visible in the case of low Ce content, while a reduction of light yield upon $AuBr_3$ addition caused by luminescence quenching phenomena is observed for high Ce concentration.

1 Introduction

The ability of inorganic scintillators to efficiently emit visible or ultraviolet light as they are struck by ionizing radiation (be it high energy photons or particles) makes these materials fundamental in medical, industrial, high energy physics and astronomy, as well as security applications.[1–3] The wide variety of ionizing radiation in terms of energy, type, and flux used in the various applications implies that no single scintillator is able to meet the specific requirements of all applications. For this reason, scintillators are currently the subject of intense research and development (R&D) efforts, concentrated on both the discovery of new materials and the optimization of the established ones.[4,5]

The light emission from a scintillator is in fact the last of a complex series of events occurring after the initial interaction of ionizing radiation with the material. Free charge carrier thermalization and their transfer to the luminescence centers, in particular, can be strongly affected by the presence of defects acting as traps for the carriers. The competition between charge carrier recombination and trapping is ultimately responsible for the degradation of the scintillator response with a reduction in the light yield, the presence of long scintillation decay tails and afterglow, and luminescence hysteresis phenomena.[6–8] Many R&D efforts are indeed dedicated to the minimization of the impact of defects on the final light emission from scintillators.

Several synthesis strategies, from aliovalent (co-)doping[9–12] to band gap engineering and solid solution,[13–16] have been reported over time to deal with defects in scintillators. In this context, we reported the use of $AuBr_3$ as additive in the melt during the growth of BaBrCl:Eu single crystals.[17] This additive strongly improves the scintillation characteristics of BaBrCl:Eu with light yield increases up to 3 times and remarkable reductions in long scintillation tails; these improvements are accompanied by a clear reduction in thermally and optically stimulated features related to halide vacancies. In a later paper[18] we reported picosecond transient absorption measurements which indicate that the addition of $AuBr_3$ reduces the concentration of native halide vacancies that can capture electrons to form F centers. Moreover, the reduction of halide vacancies and their effect in breaking up electron–hole pairs created by ionizing radiation suppresses the slow self-trapped holes migration and tunneling process involved in the BaBrCl:Eu scintillation to the benefit of prompt formation of self-trapped excitons followed by the picosecond-scale dipole–dipole energy transfer toward Eu^{2+} ions. $AuBr_3$ mechanism in the reduction of halide vacancies is not

Lawrence Berkeley National Laboratory, One Cyclotron road, Berkeley, CA 94720, USA. E-mail: fmoretti@lbl.gov, yuan.dongsheng@nims.go.jp

† Present address: National Institute for Materials Science (NIMS), 1-1 Namiki, Tsukuba, Ibaraki 305-0044, Japan.

fully clear, however no Au could be detected in the crystals and it clearly segregates as pure gold rejected on top of the boules at the end of the growth process.[18] Therefore, there are clear indications that its effect is related to the low thermal stability of this compound leading to its dissociation in metallic gold and bromine gas.[19,20] The presence of Br_2 gas in the sealed ampoules in which the crystals are grown reduces the probability of having Br evaporation from the melt and thus minimizes the concentration of halide vacancies.

In this paper we expand our study on the possible use of $AuBr_3$ as an additive to the melt for two other different Br-based scintillators, $BaBr_2$:Eu and $Cs_2LiLaBr_6$:Ce, with the aim to understand the applicability of such a technique to other bromides. The chosen compounds are characterized by very different melting temperatures (857 °C and 490 °C for $BaBr_2$ and $Cs_2LiLaBr_6$, respectively) and different activators (Eu^{2+} and Ce^{3+}).

$Cs_2LiLaBr_6$:Ce is a member of the elpasolite crystal family and has good scintillation properties (about 50 000 ph per MeV, and energy resolution of 2.9% at 663 keV).[21] The possibility of enriching it with ^6Li has also been exploited in order to obtain both thermal neutron and γ radiation detection and identification using pulse shape discrimination techniques.[22–24] $Cs_2LiLaBr_6$:Ce is commercially available.[25]

$BaBr_2$:Eu has been reported as a scintillator about a decade ago[26] showing rather interesting scintillation properties. More recent studies[27,28] on this material note that, despite the encouraging light yield and energy resolution (about 49 000 ph per MeV and 6.9% at 663 keV), $BaBr_2$ performance is far from the theoretical limit.

2. Experimental

$BaBr_2$ and $Cs_2LiLaBr_6$ single crystals were grown by the Bridgman Stockbarger method in evacuated sealed quartz ampoules using high purity (99.999%) $BaBr_2$, CsBr, LiBr, $LaBr_3$, $EuBr_2$, $CeBr_3$, and $AuBr_3$ beads from Sigma Aldrich. $BaBr_2$:Eu crystals were grown with a nominal Eu concentration in the melt ranging from 0.5 mol% to 8 mol%. $Cs_2LiLa_{1-x}Ce_xBr_6$ crystals were grown starting from stoichiometric mixtures of the raw materials and with Ce concentrations x equal to 0.005 and 0.2, these two concentrations will be called throughout the paper as 0.5 and 20 mol% Ce. Two sets of crystals with and without $AuBr_3$ (0.05 mol% with respect to La or Ba) as additive to the melt were grown. Considering the hygroscopic nature of both the raw materials and the obtained crystals, all handling was performed in an Ar-filled glove box maintained below 0.1 ppm of O_2 and H_2O. Prior to ampoule sealing, the raw materials were heated up to 110 °C and kept under vacuum for at least 24 h. All crystals were grown at a rate of 1 mm h^{-1}.

Phase identification was performed by powder X-ray diffraction using a Bruker Nonius FR591 X-ray tube using Cu Kα radiation and a MAR plate detector. Parts of the obtained samples were later crushed into smaller pieces (with dimensions ranging from 0.2 to 2 mm) and put into gas tight quartz cuvettes (internal diameter 4 mm, length 35 mm) for the optical characterization.[29,30]

Pulse height spectra were obtained by exciting the samples with a ^{137}Cs γ-ray source (E = 662 keV) with a Hamamatsu R6231-100 photomultiplier (PMT) connected to a Canberra 2005 preamplifier, a Canberra 2022 shaping amplifier and an Ortec EASY-MCA-8K multichannel analyzer. The PMT voltage was set to 700 V. The samples were optically coupled to the PMT window with silicone grease (Viscasil 600000) and covered with several layers of PTFE. The photopeak position and full width at half maximum (FWHM) were evaluated from the obtained spectra by fit in term of Gaussian component(s) taking into consideration also the presence of possible satellite peaks related to the escape of characteristics X-rays. The absolute number of photons emitted per MeV was estimated by comparing the response of a NaI:Tl (5 × 5 × 2 mm) single crystal to those of $BaBr_2$:Eu and $Cs_2LiLaBr_6$:Ce taking into consideration the PMT quantum efficiency. The light output of NaI:Tl was assumed to be 40 000 ph per MeV.

Room temperature (RT) radioluminescence (RL) measurements were obtained using a rotating copper anode X-ray generator (Bruker FR591) operated at 50 kV and 60 mA as excitation source. The emitted light is collected by a SpectraPro-2150i spectrometer (Acton Research) coupled to a PIXIS:100B CCD detector (Princeton Instruments).[30] The obtained spectra have been corrected for the instrument spectral response. The same setup was used to obtained thermally stimulated luminescence (TSL) measurements in the 10–380 K interval after irradiation of the sample at 10 K for 30 minutes. The heating rate was set to 0.1 K s^{-1} for $BaBr_2$ crystals and to 0.08 K s^{-1} in the case of $Cs_2LiLaBr_6$ ones. Sample cooling and heating was done through an Advanced Research System cryocooler and with a Lakeshore 336 temperature controller. Considering the presence of the quartz cuvette and the unequal size of the crystal pieces inside them, TSL glow curves should be considered more qualitative than quantitative in nature.

A custom build pulsed X-ray system working in time correlated single photon counting and consisting of a light-excited X-ray tube (Hamamatsu N5084) driven by an ultrafast Ti:Sapphire laser (200 fs pulses, Coherent Mira), a Hamamatsu multichannel plate photomultiplier (R3809U-50) was used to collect scintillation decay measurements. No wavelength discrimination was used to select the light emitted by the samples. The signal is processed through an Ortec 9308 ps analyzer. The overall instrument response function of the system is of the order of 100 ps FWHM.[31] The decay times were determined from the experimental results using the method described in ref. 32.

3. Results

3.1 Crystal growth

All the grown crystals appear transparent, although with cracks. Similarly to what detected in the case of BaBrCl single crystals grown with $AuBr_3$ as an additive,[18] the $BaBr_2$ and the $Cs_2LiLaBr_6$ samples show the presence of molecular bromine on the top part of the ampoules prior to their opening. The orange coloration of

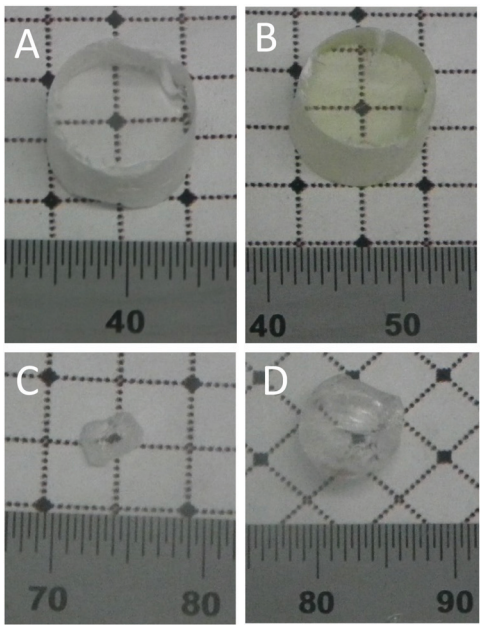

Fig. 1 Photographs of $Cs_2LiLaBr_6$:0.5 mol% Ce single crystals obtained without (A) and with (B) $AuBr_3$ additive. Panel (C) and (D) are for $BaBr_2$: 5 mol% Eu without and with $AuBr_3$, respectively. The two $BaBr_2$ samples have not been polished to an optical grade. The scale in the pictures is in mm.

the ampoule is, however, less evident than that seen in the case of BaBrCl samples due to the lower concentration of $AuBr_3$ used in this work. Fig. 1 presents pictures of representative single crystal pieces. Panel A and B show polished single crystal pieces of $Cs_2LiLaBr_6$:0.5 mol% Ce without (panel A) and with (B) the $AuBr_3$ addition. It has to be noted that all the $Cs_2LiLaBr_6$ crystals grown with $AuBr_3$ appear slightly yellow. The nature of this coloration is not clear, at the moment, and we cannot exclude that it might be related to the inclusion in the crystal of Au ions or bromine excess.

Panel C and D of Fig. 1 present photographs of $BaBr_2$: 5 mol% Eu single crystals without and with, respectively, the addition of $AuBr_3$. In this case the crystal pieces have not been lapped or polished to an optical finish. No coloration of the crystal is visible upon $AuBr_3$ addition.

3.2 Radioluminescence results

Fig. 2 reports the normalized RL spectra of $BaBr_2$:Eu crystals as a function of the Eu concentration as well as with and without $AuBr_3$ as an additive to the melt. The spectra are characterized by a bright luminescence centered at about 3.05 eV due to the typical Eu^{2+} radiative recombination between 5d and 4f levels in barium halide crystals.[16,27] The emission maximum position shifts slightly toward lower energies as the Eu content is increased; this shift is related to reabsorption of the emitted light. Also, a close comparison between the spectra of the samples obtained with and without $AuBr_3$ addition evidences small shape variations in the RL spectra (particularly on the high energy side of the emission of the two highest Eu concentrations). These slight changes in shape are possibly related to somewhat different actual Eu content in the two sets of crystals, and to the

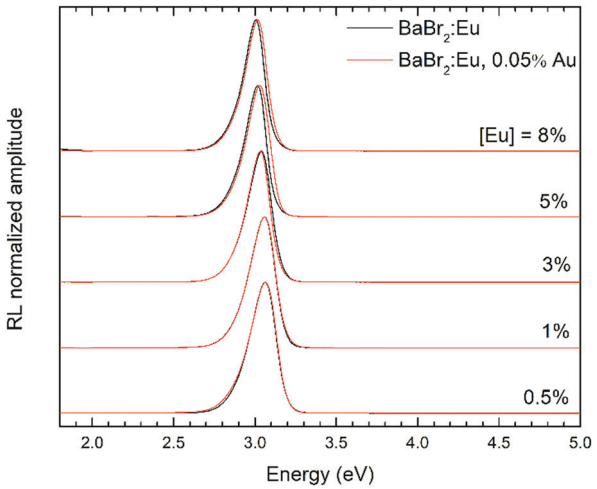

Fig. 2 Normalized RL spectra of $BaBr_2$:Eu and $BaBr_2$:Eu,Au as a function of Eu concentration. The spectra have been normalized at their maximum and shifted along the ordinate axis for clarity.

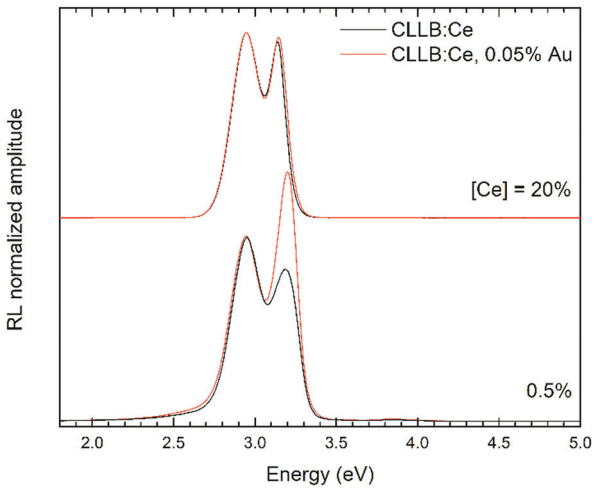

Fig. 3 Normalized RL spectra of $Cs_2LiLaBr_6$:Ce and $Cs_2LiLaBr_6$:Ce,Au as a function of Ce concentration. The spectra have been normalized at the 2.95 eV maximum and shifted along the ordinate axis for clarity.

related reabsorption role in shaping the RL spectra. These slight changes in shape do not seem, though, particularly relevant considering the below presented results.

The RL spectra of $Cs_2LiLaBr_6$:Ce, both as a function of the Ce concentration and of the $AuBr_3$ addition, are reported in Fig. 3. All the spectra are characterized by the Ce^{3+} emission doublet, due to transition between 5d and 4f ($^2F_{5/2}$ and $^2F_{7/2}$) ground state levels, with maximum at about 2.9 and at about 3.2 eV, and in good agreement with previously published results.[21] As expected, the higher energy emission component is affected by the increase in Ce^{3+} concentration, with a clear shift in its position from 3.2 down to 3.15 eV and a slightly lower FWHM. These changes in shape are related to reabsorption of the emitted light. In the case of the $Cs_2LiLaBr_6$ samples doped with 0.5 mol% Ce, the main emission is also accompanied by a weaker component on the low energy side and appearing as a long

tail. This latter component is possibly related to defect emission or to (self-) trapped excitons. In the case of the 20 mol% $Cs_2LiLaBr_6$:Ce samples, there are no evident variations in the emission shape as the addition of $AuBr_3$ is considered; on the contrary, for the samples grown with the lower Ce content, there is a clear change in the ratio between the two Ce^{3+} emission components. It is not clear, at the moment, what are the reasons behind this amplitude reversal upon the use of $AuBr_3$.

3.3 Pulsed X-ray decays

RT scintillation decay kinetics of both $BaBr_2$ and $Cs_2LiLaBr_6$ with and without $AuBr_3$ and for different Eu or Ce concentrations have been studied with pulsed X-rays. Fig. 4 presents the results obtained for $BaBr_2$:Eu for two different Eu concentrations (namely, 0.5 and 8 mol%) as representative of the observed phenomenology. In the case of the 0.5 mol% Eu sample the decay is characterized by a two exponential decay components of about 450 and 860 ns (accounting for 38 and 9% of the decay area), and by a much longer contribution, appearing as a constant in the reported timescale and representing decay time components longer than 10 μs, which accounts for the remaining 53% of the emitted light. As the Eu concentration is increased, the decays still maintain a double exponential decay character (though the fit decay times and their relative ratio change) but the weight of the constant fraction becomes less and less evident until it reaches about 8% for the highest Eu concentration considered. The introduction of $AuBr_3$ does not significantly change the time decay components, but has a strong influence on the detected constant fraction, which decreases to 51% in the case of 0.5 mol% Eu sample and to less than 1% for the 8 mol% Eu samples. So, in the case of $BaBr_2$ the addition of $AuBr_3$ results in a lower fraction of delayed light similarly to what was reported for BaBrCl:Eu single crystals,[17] and clearly suggesting a reduced role of charge carrier trapping states in the scintillation phenomenon.

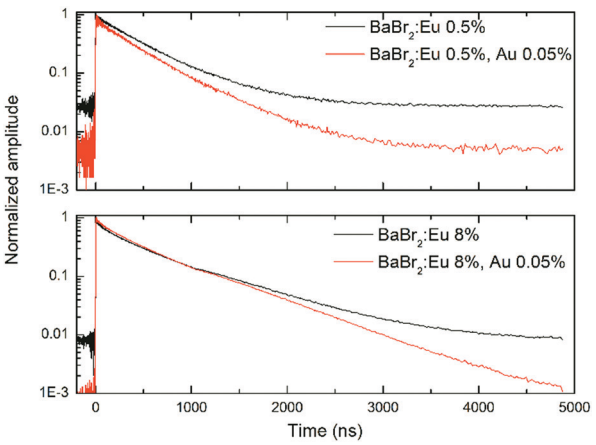

Fig. 4 Pulsed X-ray decays of $BaBr_2$:Eu without and with $AuBr_3$ addition in the melt for two different Eu concentrations, reported in the figure legends. The instrument background of each measurement has been subtracted before normalization.

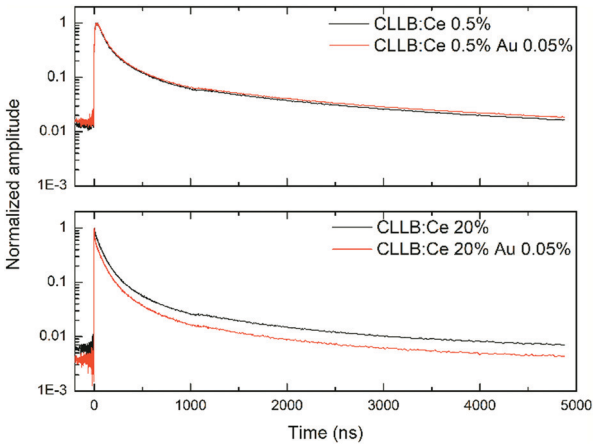

Fig. 5 Normalized pulsed X-ray decays of $Cs_2LiLaBr_6$:Ce for two different Ce concentrations, reported in the figure legend, and considering the addition of $AuBr_3$ in the melt. The instrument background has been subtracted before normalization.

The pulsed X-ray decays obtained in the case of the $Cs_2LiLaBr_6$:Ce crystals, Fig. 5, present a very different phenomenology, with no substantial impact of $AuBr_3$ on the decay kinetics of $Cs_2LiLaBr_6$:Ce. In fact, the decays always appear similar to those already reported in the literature,[21] with three decay components (about 60 ns, 200 ns, >1000 ns) and a constant fraction. The intensity ratios of the components are only affected by the Ce concentration. The only discrepancy is visible exclusively for the 20 mol% Ce with $AuBr_3$ which shows a further minor component of about 5 ns, absent in the case of the crystal obtained without $AuBr_3$. This very fast component might indicate the presence of luminescence quenching phenomena. In any case, the constant fraction has substantially the same overall weight, independently from the amount of Ce and the addition of $AuBr_3$ in the synthesis.

3.4 Thermally stimulated luminescence

TSL measurements in the 18–380 K interval were performed to add evidence to the effect of $AuBr_3$ addition in the melt on the formation or inhibition of defects in the crystals. Fig. 6 compares, as an example, the glow curves obtained in the case of $BaBr_2$:0.5 mol% Eu, with and without the addition of $AuBr_3$, after irradiation with X-rays for 30 minutes at 18 K. Similar results have been obtained also for higher Eu concentrations. In both cases the glow curves are composed by two mains peaks at about 260 and 340 K accompanied by weaker and less resolved ones in the 50–200 K interval. The slight shift in the temperature of the maxima are likely related to the somewhat different thermal contact between the heater, the cuvette, and the crystal pieces contained in the cuvette itself for the two samples. The relative intensity of the peaks, however, should not be strongly affected by this phenomenon. The comparison between the two glow curves clearly evidences the remarkable reduction in the intensity ratio between the 340 and the 260 K glow peaks upon the addition of $AuBr_3$ in the melt. This is also very similar to what has been reported in the case of

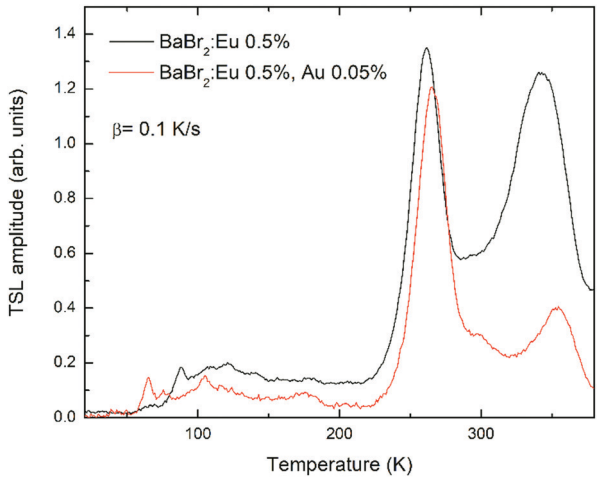

Fig. 6 TSL glow curve of $BaBr_2$:0.5 mol% Eu with and without $AuBr_3$ addition. The curves have been obtained after integration on the Eu^{2+} emission region (2.80–3.22 eV) of the wavelength resolved data. The heating rate was set to 0.1 K s^{-1}.

BaBrCl:Eu,[17] suggesting that also in the case of $BaBr_2$ the addition of $AuBr_3$ is able to reduce the amount of defect states likely related to native halide vacancies.

The TSL results obtained for the $Cs_2LiLaBr_6$ samples show, again, a different behavior upon $AuBr_3$ addition compared to $BaBr_2$:Eu. In the $Cs_2LiLaBr_6$ case, the glow curves (Fig. 7, where the results for the samples doped with 0.5 mol% Ce are reported) are composed by 5 main peaks all in the 10–200 K interval whose relative amplitude does not seem to be clearly affected by $AuBr_3$. On the other hand, the sample obtained with $AuBr_3$ is clearly characterized by a higher general intensity in the glow peaks compared to the one without, suggesting that the addition of $AuBr_3$ might increase the defect concentration of $Cs_2LiLaBr_6$.

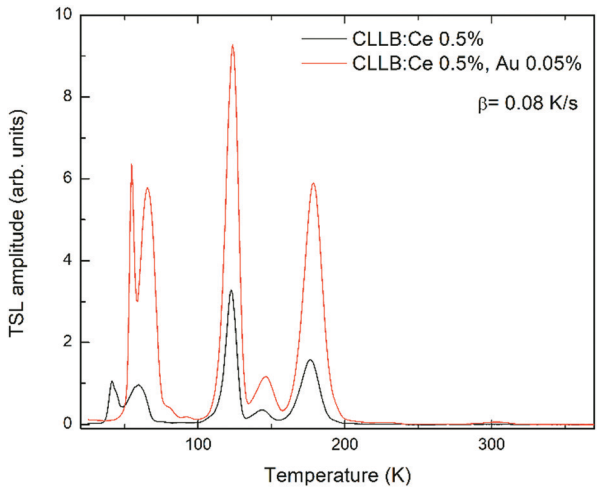

Fig. 7 TSL glow curves of $Cs_2LiLaBr_6$:0.5 mol% Ce with and without $AuBr_3$ addition. The curves have been obtained from wavelength resolved results by integration on the Ce^{3+} emission (2.80–3.34 eV). Heating rate 0.08 K s^{-1}.

3.5 Scintillation light yield and non-proportionality

Pulse height spectra for the $BaBr_2$:5 mol% Eu crystals, both with and without the addition of $AuBr_3$, are reported in Fig. 8 as an example of the observed phenomenology in the entire Eu concentration range. The spectra show clearly the presence of photopeaks with a shoulder at lower channel position related to the escape of characteristics X-rays. $AuBr_3$ clearly affects the position of the photoelectric peak, which is shifted from channel 3600 to 6500, indicating an overall increase in the light yield of $BaBr_2$ by a factor close to 1.7. The calculated light yield (LY) and energy resolution (ER) of the entire Eu concentration series are reported in Fig. 9A and B, respectively. The light yield of $BaBr_2$:Eu increases from 6800 up to 40 000 ph per MeV as the europium concentration is increased from 0.5 to 8 mol%. The addition of $AuBr_3$ leads to a systematic improvement of the

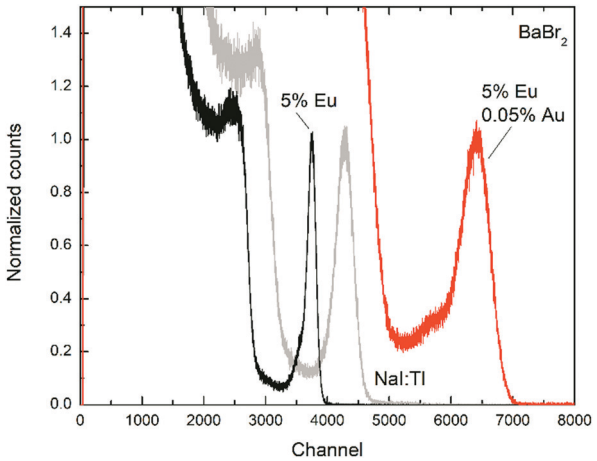

Fig. 8 Pulse height spectra obtained on $BaBr_2$:0.5 mol% Eu with and without the addition of $AuBr_3$ by using a ^{137}Cs (662 keV) γ-source. The spectrum of a NaI:Tl crystal is also reported as a reference.

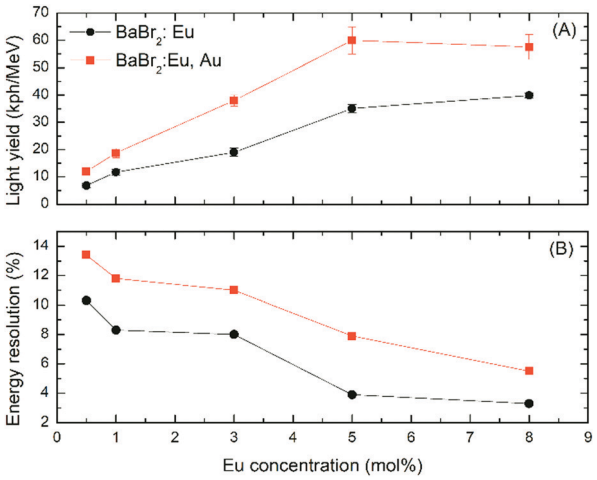

Fig. 9 Light yield (panel A) and energy resolution (panel B) calculated from the pulse height spectra of $BaBr_2$:Eu as a function of Eu concentration and $AuBr_3$ presence during crystal growth. The lines are only a guide for the eyes.

detected light yield for the entire Eu concentration series. These improvements are in the 1.4 to 2 times range and do not seem to be clearly dependent on the Eu concentration, on the contrary to what was observed in the case of BaBrCl:Eu in which the improvement was particularly evident at low Eu contents.[17] The reason behind the different behavior between LY improvements, and their relative amount as well, detected for BaBrCl and $BaBr_2$ might be related to the expected lower thermal stability of F centers of the latter compound with respect to the former. Considering the above reported results, the increased light yield of the crystals grown with $AuBr_3$ is likely related to the reduction in long scintillation decay tails and thus to a lower concentration of defects and notably in the reduction of native halide vacancy presence.

Quite unexpectedly, considering the improved light yield, the energy resolution of the $BaBr_2$:Eu samples (Fig. 9B) grown with $AuBr_3$ is clearly worse for the entire europium concentration range, indicating that the measured ER is not dominated by the photo-electron statistics. In order to understand why the samples grown with $AuBr_3$ are characterized by a worse ER, LY non-proportionality measurements have been performed on the two $BaBr_2$:5 mol% Ce. The results, reported in Fig. 10, clearly evidence the much lower proportionality – with deviations up to 13% – of the sample synthesized with $AuBr_3$. The lower proportionality of the sample obtained with $AuBr_3$ and the related larger fluctuations in the number of emitted photons are responsible for the reduced energy resolution detected for this crystal compared to the one obtained without $AuBr_3$.

Fig. 11 reports the pulse height spectra obtained on the $Cs_2LiLaBr_6$:Ce samples as a function of both Ce concentration and presence of $AuBr_3$ during the growth. In the case of low Ce concentration, the light yield of $Cs_2LiLaBr_6$ does not seem to be appreciably modified by the presence of $AuBr_3$, since the small shift in the position of the photopeak toward lower channel

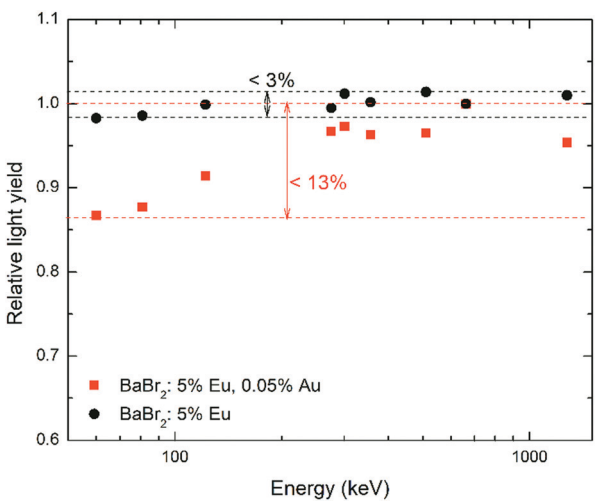

Fig. 10 Relative light yield of $BaBr_2$:5 mol% Eu with and without the addition of $AuBr_3$ in the ampoule as a function of the excitation energy. The data have been obtained from fits in terms of Gaussian components of the photoelectric peaks detected by exciting the samples with different radioactive sources. The data have been normalized at 662 keV.

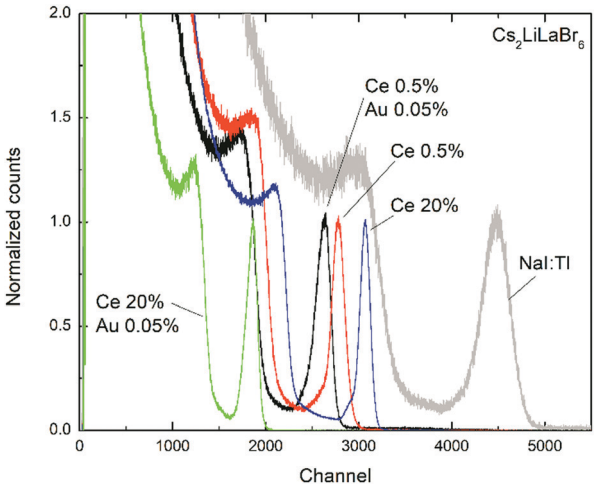

Fig. 11 Normalized pulse height spectra of $Cs_2LiLaBr_6$:Ce and $Cs_2LiLaBr_6$:Ce,Au for different Ce concentrations. Spectra have been obtained by using ^{137}Cs 662 keV γ-photons. The NaI:Tl spectrum is reported as well as a reference.

numbers is consistent with the typical errors encountered with this kind of measurements. The calculated light yields are of the order of 29 000 and 27 000 ph per MeV with energy resolution of about 6 and 7% for the sample obtained without and with $AuBr_3$, respectively. In the case of the highly Ce doped samples, however, there is a remarkable reduction in the photopeak position as $AuBr_3$ is added to the melt. The calculated LY decreases from 38 000 to 20 000 ph per MeV and is also accompanied by a significant worsening of the energy resolution from 4 to 6%. At the moment it is not clear why this is happening, though it might partly be related to the presence of the very fast scintillation contribution reported above in the discussion of Fig. 4. The yellow coloration of the samples grown with gold tri-bromide might have a role as well.

Fig. 12 reports the non-proportionality measurements obtained on the $Cs_2LiLaCl_6$:0.5 mol% Ce with and without the addition of $AuBr_3$. The comparison of the two non-proportionality curves clearly evidences a worse response as a function of the γ-ray photon energy for the sample obtained with $AuBr_3$.

4. Discussion

Considering the just presented results, the impact of the presence of $AuBr_3$ in the melt during crystal growth of $Cs_2LiLaBr_6$:Ce and of $BaBr_2$:Eu is very different. The large improvements in both light yield and timing detected upon $AuBr_3$ addition in the case of $BaBr_2$:Eu are substantially related to the lower concentration of native defects and notably of halide vacancies, as evidenced by the TSL results, and are coherent with the results previously reported for BaBrCl:Eu single crystals.[17] On the contrary, $AuBr_3$ not only does not improve the scintillation characteristics of $Cs_2LiLaBr_6$:Ce but might be the cause of reduced performance. Preliminary first principles calculations suggest that the halide vacancy formation energy is not substantially different between $BaBr_2$ and $Cs_2LiLaBr_6$,

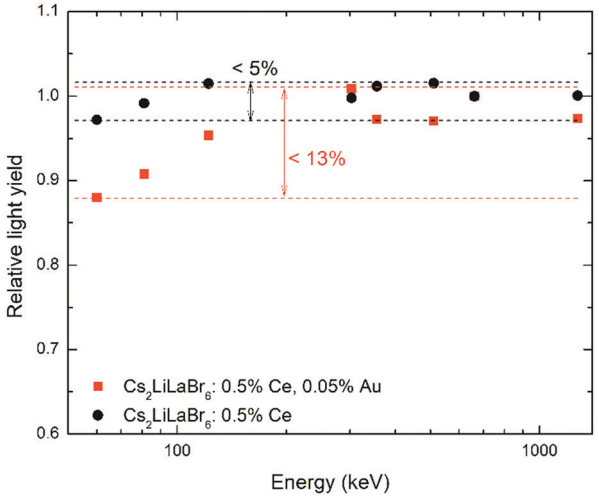

Fig. 12 Relative light yield of $Cs_2LiLaBr_6$:0.5 mol% Ce with and without the addition of $AuBr_3$ in the ampule as a function of the excitation energy. The data have been obtained from fits in terms of Gaussian components of the photopeak detected by exciting the samples with different radioactive sources. The data have been normalized at 662 keV.

so the very different behavior upon $AuBr_3$ addition is possibly related to the much lower melting temperature of $Cs_2LiLaBr_6$, with respect to the two other Ba halides, and thus to a lower formation probability of halide vacancies.

The unexpected lower energy resolution of $BaBr_2$:Eu and the related worse non-proportionality, reported in Fig. 9 and 10, require some explanations. While going into the opposite direction, these results are believed to be related to those obtained for $LaBr_3$:Ce and $CeBr_3$ crystals co-doped with Sr^{2+} or Ca^{2+}.[11,33–36] The addition of these aliovalent ions results in a more proportional light yield energy response, and thus in better energy resolution, but it also introduces extra Br vacancies for charge compensation. First principles calculations[37,38] showed that these Br vacancies are bound to the alkali earth ions resulting in stable neutral defect complexes and that the vacancy energy levels are shifted closer to the conduction band edge with respect to those of the isolated Br vacancies. These co-dopant-bound halide vacancies do trap electrons, but the resulting F_A centers are shallow traps and, at room temperature, they give rise to scintillation decay tails of the order of only few μs,[33] thus not affecting the LY. Moreover, it has been suggested[33,38] that this temporary electron trapping is effectively reducing the free electron density resulting in a decrease in the probability of Auger quenching of electron–hole pairs occurring during carrier thermalization and transfer toward the luminescent centers. This results in lower fluctuations in the photon statistics and improved non-proportionality.

We suggest that something similar is at play also in the case of $BaBr_2$:Eu samples reported here. However, the *F* centers in $BaBr_2$:Eu are rather deep traps – as evidenced by the position in temperature of the glow peaks reported in Fig. 5 compared to the ones which appear in the case of $LaBr_3$:Ce reported in ref. 27 – with a much longer decay time than that of the F_A centers in $LaBr_3$:Ce,Sr. As a result, electrons remain trapped on the F centers for an extended period of time, longer than the shaping time used in our LY measurements, and thus in the low light yields reported in Fig. 9. So, as we remove the halide vacancies in $BaBr_2$, and BaBrCl, by adding $AuBr_3$ in the melt, we are increasing the light yield but, at the same time, we are also increasing the probability of non-linear quenching phenomena related to the higher concentration of free carriers. In this sense it seems to us that the $LaBr_3$ and $BaBr_2$ cases are pretty similar. The discriminating factor between the effect of the halide vacancies in the two matrices on light yield, non-proportionality, and non-linear quenching phenomena is the different thermal stability that these traps have in $LaBr_3$ and in $BaBr_2$: in the former case where the trap energy is small, the time spent by electrons as trapped charges on the codopant-bound halide vacancies is sufficient to reduce the non-linear quenching phenomenon probability but not long enough to affect the light yield of the material. On the contrary in the case of $BaBr_2$, where the trap energy is significantly larger, the electrons trapped on the vacancies are effectively not participating to the scintillation process and, instead, likely contribute to the afterglow. This trapping, however, still helps in reducing the probability of non-linear quenching processes.

In summary, by reducing the concentration of Br vacancies, the $AuBr_3$ addition during crystal growth has indeed the positive effect of reducing the amount of electron that cannot participate in a timely manner in the scintillation process but at the cost of a higher probability of quenching phenomena, resulting in the more evident energy response non-proportionality of the crystals.

As a more general note, these results raise interesting questions to our current understanding of the defect role in the scintillation process. On one side, it is very well recognized that defects which trap charge carriers for extended periods of time have a negative effect on the scintillator performances. On the other, the results presented here, as well as those on $LaBr_3$:Ce and $CeBr_3$ and on alkali earth codoped garnets and silicates,[3,5] suggest that in some cases defects can also intervene in the scintillation process in a substantially positive way. What is not currently understood is which combination of defect parameters (energy, type, concentration), recombination processes (consecutive charge carrier or excitonic recombination), electron/hole track structure and density, as well as charge carrier thermalization length might lead to a generally positive role of defects on the scintillation process. A hint at needed complex co-doping strategies was shown for NaI:Tl,Eu,Ca, a combination that increased both the light yield and the energy resolution.[12] As such, a more complete understanding on the defect role might lead to novel ways to improve the performances of scintillators which go beyond the currently employed strategies of pure mitigation and reduction of the defect presence.

5. Conclusions

The introduction of $AuBr_3$ in the growth ampoules of $BaBr_2$:Eu and $Cs_2LiLaBr_6$:Ce as an additive in the melt to increase the scintillation properties of these crystals gives mixed results.

In the case of $Cs_2LiLaBr_6$:Ce no improvements were detected, and in the case of highly Ce-doped crystals this additive lead to a decrease in the scintillation light yield. In the case of $BaBr_2$:Eu, on the other hand, clear improvements up to two times in the light yield and reductions in the long lived scintillation decay tails were clearly visible. These improvements are related, as in the case of BaBrCl:Eu crystals, to the reduction in the concentration of native halide vacancies. However, these higher light yields are accompanied by worse energy resolution for the entire series of Eu concentration. The worse energy resolution is likely related to an increased probability in Auger quenching of electron/hole pairs before their recombination to the luminescent center, leading us to believe that, although the electron trapping at the halide vacancies forming F centers is responsible for the degraded scintillation properties of the crystals obtained without $AuBr_3$, the trapping might also have the positive role of decreasing the free carrier concentration, thus reducing the probability of non-linear quenching phenomena. A similar mechanism has been suggested also in the case of the improvements in both light yield and energy resolution in Sr or Ca codoped $LaBr_3$ and $CeBr_3$. Finally, these results clearly put in further evidence the very complex role of defects in the scintillation process.

Author's contribution

FM: Conceptualization, Investigation (supporting), Visualization (equal), Writing-original draft (lead), Writing-review and editing (equal); DY: Investigation (lead), Data curation, Visualization (equal); DP: Investigation (supporting); EB: Project administration, Conceptualization, Funding acquisition, Writing-review and editing (equal).

Conflicts of interest

There are no conflicts to declare.

Acknowledgements

This work was supported by the US Department of Energy/NNSA/DNN R&D and carried out at Lawrence Berkeley National Laboratory under contract No. AC02-05CH11231. The authors would also like to acknowledge prof. S. E. Derenzo for useful discussions.

Notes and references

1 P. Lecoq, A. Gektin and M. Korzhik, *Inorganic scintillators for detector systems*, Springer Verlag, Berlin, 2006.
2 P. Rodnyi, *Physical processes in inorganic scintillators*, CRC Press, Boca Raton, FL, 1997.
3 C. Dujardin, E. Auffray, E. Bourret-Courchesne, P. Dorenbos, P. Lecoq, M. Nikl, A. N. Vasil'ev, A. Yoshikawa and R.-Y. Zhu, Needs, Trends, and Advances in inorganic scintillators, *IEEE Trans. Nucl. Sci.*, 2018, **65**, 1977–1997.
4 S. E. Derenzo, M. J. Weber, E. Bourret-Courchesne and M. K. Klintenberg, The quest for the ideal inorganic scintillator, *Nucl. Instrum. Methods Phys. Res., Sect. A*, 2003, **505**, 111–117.
5 M. Nikl and A. Yoshikawa, Recent R&D trends in inorganic single-crystal scintillator materials for radiation detection, *Adv. Opt. Mater.*, 2015, **3**, 463–481.
6 M. Nikl, V. V. Laguta and A. Vedda, Complex Oxide scintillators: materials defects and scintillation performance, *Phys. Status Solidi B*, 2008, **245**, 1701–1722.
7 E. Dell'Orto, M. Fasoli, G. Ren and A. Vedda, Defect-driven radioluminescence sensitization in scintillators: the case of $Lu_2Si_2O_7$:Pr, *J. Phys. Chem. C*, 2013, **117**, 20201–20208.
8 F. Moretti, G. Patton, A. Belsky, M. Fasoli, A. Vedda, M. Trevisani, M. Bettinelli and C. Dujardin, Radioluminescence sensitization in scintillators and Phosphors: trap engineering and modeling, *J. Phys. Chem. C*, 2014, **118**, 9670–9676.
9 M. Nikl, P. Bohacek, K. Nitsch, E. Mihokova, M. Martini, A. Vedda, S. Croci, G. P. Pazzi, P. Fabeni, S. Baccaro, B. Borgia, I. Dafinei, M. Diemoz, G. Organtini, E. Auffray and P. Lecoq, Decay kinetics and thermoluminescence of $PbWO_4$:La^{3+}, *Appl. Phys. Lett.*, 1997, **71**, 3755.
10 M. A. Spurrier, P. Szupryczynski, K. Yang, A. A. Carey and C. Melcher, Effects of Ca^{2+} co-doping on the scintillation properties of LSO:Ce, *IEEE Trans. Nucl. Sci.*, 2008, **55**, 1178–1182.
11 P. Guss, M. E. Foster, B. M. Wong, F. P. Doty, K. Shah, M. R. Squillante, U. Shirwadkar, R. Hawrami, J. Tower and D. Yuan, Results for aliovalent doping of $CeBr_3$ with Ca^{2+}, *J. Appl. Phys.*, 2014, **115**, 034908.
12 I. V. Khodyuk, S. A. Messina, T. J. Hayden, E. D. Bourret and G. A. Bizarri, Optimization of scintillation performance *via* a combinatorial multi-element co-doping strategy: application to NaI:Tl, *J. Appl. Phys.*, 2015, **118**, 084901.
13 O. Sidletskiy, Trends in search of bright mixed scintillators, *Phys. Status Solidi A*, 2018, **215**, 170103.
14 K. Kamada, T. Endo, K. Tsutumi, T. Yanagida, Y. Fujimoto, A. Fukabori, A. Yoshikawa, J. Pejchal and M. Nikl, Composition engineering in cerium-doped $(Lu,Gd)_3(Ga,Al)_5O_{12}$ single-crystal scintillators, *Cryst. Growth Des.*, 2011, **11**, 4484–4490.
15 M. Fasoli, A. Vedda, M. Nikl, C. Jiang, B. P. Uberuaga, D. A. Andersson, K. J. McClellan and C. R. Stanek, Band-gap engineering for removing shallow traps in rare-earth $Lu_3Al_5O_{12}$ garnet scintillators using Ga^{3+} doping, *Phys. Rev. B: Condens. Matter Mater. Phys.*, 2011, **84**, 081102(R).
16 G. Gundiah, Z. Yan, G. Bizarri, S. E. Derenzo and E. D. Bourret-Courchesne, Structure and scintillation of Eu^{2+}-activated BaBrCl and solid solutions in the $BaCl_2$–$BaBr_2$ system, *J. Lumin.*, 2013, **138**, 143–149.
17 T. Shalapska, F. Moretti, E. Bourret and G. Bizarri, Effect of Au codoping on the scintillation properties of BaBrCl:Eu single crystals, *J. Lumin.*, 2018, **202**, 497–501.
18 P. Li, S. Gridin, K. B. Ucer, R. T. Williams, M. Del Ben, A. Canning, F. Moretti and E. Bourret, Picosecond absorption spectroscopy of excited states in BaBrCl with and without Eu dopant and Au codopant, *Phys. Rev. Appl.*, 2019, **12**, 014035.
19 *Handbook of Chemistry and Physics*, ed. J. R. Rumble, CRC press, 2008.

20 http://gold.atomistry.com/auric_bromide.html.
21 U. Shirwadkar, J. Glodo, E. V. van Loef, R. Awrami, S. Mukhopadhyay, A. Churilov, W. H. Higgins and K. S. Shah, Scintillation properties of $Cs_2LiLaBr_6$:Ce (CLLB) crystals with varying Ce^{3+} concentrations, *Nucl. Instrum. Methods Phys. Res., Sect. A*, 2013, **652**, 268–270.
22 C. W. E. van Eijk, Inorganic scintillators for thermal neutron detection, *IEEE Trans. Nucl. Sci.*, 2012, **59**, 2242.
23 J. Glodo, R. Awrami, E. van Loef, U. Shirwadkar and K. Shah, Pulse shape discrimination with selected elpasolite crystals, *IEEE Trans. Nucl. Sci.*, 2012, **59**, 2328.
24 J. Glodo, E. van Loef, R. Hawrami, W. M. Higgins, A. Churilov, U. Shirwadkar and K. Shah, Selected properties of Cs_2LiYCl_6, $Cs_2LiLaCl_6$, and $Cs_2LiLaBr_6$ scintillators, *IEEE Trans. Nucl. Sci.*, 2011, **58**, 333.
25 Saint-Gobain electronic catalog, https://www.crystals.saint-gobain.com/products/cllb, last accessed: September 2020.
26 J. Selling, M. D. Birowosuto, P. Dorenbos and S. Schweizer, Europium-doped barium halide scintillators for X-ray and γ-ray detections, *J. Appl. Phys.*, 2008, **101**, 034901.
27 G. Gundiah, G. Bizarri, S. M. Hanrahan, M. J. Weber, A. D. Bourret-Courchesne and S. E. Derenzo, Structure and scintillation of Eu^{2+}-activated solid solution in the $BaBr_2$–BaI_2 system, *Nucl. Instrum. Methods Phys. Res., Sect. A*, 2011, **652**, 234–237.
28 Z. Yan, G. Gundiah, G. A. Bizarri, E. C. Samulon, S. E. Derenzo and E. D. Bourret-Courchesne, Eu^{2+}-activated $BaCl_2$, $BaBr_2$, BaI_2 scintillator revisited, *Nucl. Instrum. Methods Phys. Res., Sect. A*, 2014, **735**, 83.
29 M. Janecek, R. Borade, E. Bourret-Courchesne and S. E. Derenzo, An investigation of X-ray luminosity versus crystalline powder granularity, *Nucl. Instrum. Methods Phys. Res., Sect. A*, 2011, **659**, 252–257.
30 S. E. Derenzo, M. S. Boswell, E. D. Bourret-Courchesne, R. Boutchko, T. F. Budinger, A. Canning, S. M. Hanrahan, M. Janacek, Q. Peng, Y. Porter-Chapman, J. D. Powell, C. A. Ramsay, S. E. Taylor, l.-W. Wang, M. J. Weber and D. S. Wilson, Design and implementation of a facility for discovering new scintillator materials, *IEEE Trans. Nucl. Sci.*, 2008, **55**, 1458–1463.
31 S. E. Derenzo, M. J. Weber, W. W. Moses and C. Dujardin, Measurements of the intrinsic rise-times of common scintillators, *IEEE Trans. Nucl. Sci.*, 2000, **47**, 890.
32 S. E. Derenzo, G. A. Bizarri, E. Bourret, R. Borade, Y. Eagleman, G. Gundiah and C. Rosen, 15 lutetium compounds screened for Ce^{3+} activated scintillation, *Nucl. Instrum. Methods Phys. Res., Sect. A*, 2018, **908**, 325–332.
33 M. S. Alekhin, J. T. S. de Haas, I. V. Khodyuk, K. W. Krämer, P. R. Menge, V. Ouspenski and P. Dorenbos, Improvement of γ-ray energy resolution of $LaBr_3$:Ce^{3+} scintillation detectors by Sr^{2+} and Ca^{2+} co-doping, *Appl. Phys. Lett.*, 2013, **102**, 161915.
34 M. S. Alekhin, D. A. Biner, K. W. Krämer and P. Dorenbos, Improvement of $LaBr_3$:5%Ce scintillation properties by Li^+, Na^+, Mg^{2+}, Ca^{2+}, Sr^{2+}, and Ba^{2+} co-doping, *J. Appl. Phys.*, 2013, **113**, 224904.
35 R. H. Awater, K. W. Krämer and P. Dorenbos, Effects of Na^+, Mg^{2+}, Ca^{2+}, Sr^{2+}, and Ba^{2+} doping on the scintillation properties of $CeBr_3$, *IEEE Trans. Nucl. Sci.*, 2015, **62**, 2343.
36 F. G. A. Quarati, M. S. Alekhin, K. W. Krämer and P. Dorenbos, Co-doping of $CeBr_3$ scintillator detector for energy resolution enhancement, *Nucl. Instrum. Methods Phys. Res., Sect. A*, 2014, **735**, 655.
37 P. Erhart, B. Sadigh, A. Schleife and D. Åberg, First principle studies of codoping in lanthanum bromide, *Phys. Rev. B: Condens. Matter Mater. Phys.*, 2015, **91**, 165206.
38 P. Åberg, B. Sadigh, A. Schleife and P. Erhart, Origin of resolution enhancement by co-doping of scintillators: insight from electronic structure calculations, *Appl. Phys. Lett.*, 2014, **104**, 211908.

